Chemical Science

ROYAL SOCIETY OF CHEMISTRY

EDGE ARTICLE

View Article Online
View Journal | View Issue

Cite this: *Chem. Sci.*, 2020, **11**, 11285

All publication charges for this article have been paid for by the Royal Society of Chemistry

A molecular approach to rationally constructing specific fluorogenic substrates for the detection of acetylcholinesterase activity in live cells, mice brains and tissues†

Xiaofeng Wu,‡[a] Jong Min An,‡[b] Jizhen Shang,‡[c] Eugene Huh,‡[d] Sujie Qi,[a] Eunhye Lee,[a] Haidong Li,[a] Gyoungmi Kim,[a] Huimin Ma,[c] Myung Sook Oh,*[e] Dokyoung Kim*[bf] and Juyoung Yoon*[a]

Acetylcholinesterase (AChE) is an extremely critical hydrolase tightly associated with neurological diseases. Currently, developing specific substrates for imaging AChE activity still remains a great challenge due to the interference from butyrylcholinesterase (BChE) and carboxylesterase (CE). Herein, we propose an approach to designing specific substrates for AChE detection by combining dimethylcarbamate choline with a self-immolative scaffold. The representative **P10** can effectively eliminate the interference from CE and BChE. The high specificity of **P10** has been proved *via* imaging AChE activity in cells. Moreover, **P10** can also be used to successfully map AChE activity in different regions of a normal mouse brain, which may provide important data for AChE evaluation in clinical studies. Such a rational and effective approach can also provide a solid basis for designing probes with different properties to study AChE in biosystems and another way to design specific substrates for other enzymes.

Received 3rd August 2020
Accepted 21st September 2020

DOI: 10.1039/d0sc04213g

rsc.li/chemical-science

Introduction

Acetylcholinesterase (EC 3.1.1.7; abbreviated AChE) is a kind of enzyme that can hydrolyze neurotransmitters (*i.e.*, acetylcholine) into choline and plays a critical role in the central and peripheral nervous systems.[1–3] AChE has been considered as the main cause of neurological disorders such as Alzheimer's disease and Parkinson's disease.[4–6] Abnormal alterations in AChE activity may directly influence the function of the nervous system.[6–9] Thus, specific detection of AChE activity is still of great importance to better elucidate the function of AChE in complicated living systems, AChE-related diagnoses, and drug discovery.[9–12]

Currently, several analytical methods based on colorimetric assays,[10,11] chemiluminescence,[12] electrochemical sensors,[13,14] nanoparticles,[15] and supramolecular assemblies,[16] have been engineered to probe AChE activity. Fluorescent probes combined with fluorescence confocal imaging with unique features,[17–28] such as *in situ* and/or real-time detection, high spatiotemporal resolution and noninvasive monitoring abilities, have been extensively used in various disease diagnoses and therapies.[29,30] Currently, fluorescent probes for AChE activity analysis employ acetyl groups as recognition units.[31–39] Scheme 1A shows that, in these methods, AChE converts acetylcholine or acetylthiocholine to choline or thiocholine, respectively, which will further react with additional substrates to generate fluorescence signals. This enzyme-induced cascade reaction seriously limits its application in living systems. Another inevitable drawback is that the current substrate (*i.e.*, the acetyl group) for the detection for AChE activity always suffers from the interference of butyrylcholinesterase (BChE) and carboxylesterase (CE) due to their similar catalytic mechanism to that of AChE.[40–42] Recently, two groups proposed fluorescent probes using the dimethyl-carbamate unit for the detection of AChE activity.[43,44] However, this carbamate moiety may react with CE.[45–47] Thus, developing a general fluorogenic substrate for the specific detection of AChE remains a great challenge. We noticed that, at the base of a long and narrow 20

[a]*Department of Chemistry and Nanoscience, Ewha Womans University, Seoul 03760, Republic of Korea. E-mail: jyoon@ewha.ac.kr*

[b]*Department of Biomedical Science, Graduate School, Kyung Hee University, Seoul 02447, Republic of Korea*

[c]*Beijing National Laboratory for Molecular Sciences, Key Laboratory of Analytical Chemistry for Living Biosystems Institute of Chemistry, Chinese Academy of Sciences, Beijing 100190, China*

[d]*Department of Medical Science of Meridian, College of Korean Medicine, Graduate School, Kyung Hee University, Seoul 02447, Republic of Korea*

[e]*Department of Life and Nanopharmaceutical Sciences, Graduate School, Kyung Hee University, Seoul 02447, Republic of Korea*

[f]*Department of Anatomy and Neurobiology, College of Medicine, Kyung Hee University, Seoul 02447, Republic of Korea*

† Electronic supplementary information (ESI) available. See DOI: 10.1039/d0sc04213g

‡ These authors contributed equally to this work.

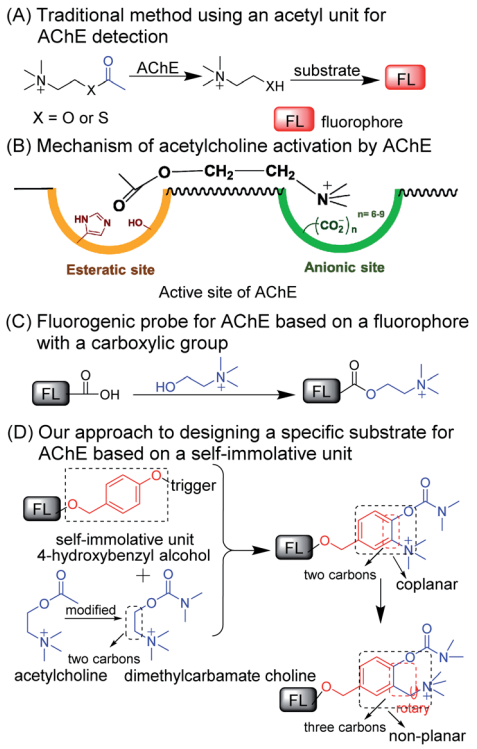

Scheme 1 The overall design of specific substrates for AChE activity. (A) Traditional method for AChE detection. (B) Binding mode of acetylcholine with the active site on AChE. (C) Fluorogenic probe for AChE detection *via* a carboxylic acid-containing fluorophore. (D) Our approach to designing a specific substrate for AChE.

Å gorge, two subunits consisted of the active site of AChE, an "esteratic" subsite containing the catalytic machinery, and an "anionic" subsite that can bind to the quaternary ammonium group, resulting in an increased affinity ability between AChE and the ammonium group (Scheme 1B).[48,49] These data suggest that the two following criteria may be considered and incorporated into the design of a specific substrate toward AChE: (i) the substrate should have an alkylated ammonium group, and (ii) a distance of two or three C–C bonds should be kept between the ammonium group and the recognition moiety.[2,48,49]

The resulting key issue is determining how to connect and combine the recognition unit with a two- or three-carbon alkylated ammonium group to fluorophore in one molecule. One easy way to achieve this is to make such a probe for AChE by directly incorporating choline into a carboxylic acid-containing fluorophore (Scheme 1C). However, currently, few such fluorophores can achieve signal conversion before and after the reaction. Thus, we shift our attention to a self-immolative scaffold (*i.e.*, 4-hydroxybenzyl alcohol) that has been used as an excellent linker connecting recognition units to fluorophores.[50,51] As shown in Scheme 1D, the commonly used carbamate for AChE was employed to revise choline which could be incorporated into the self-immolative linker as a substrate for AChE and then this whole structure can be connected to a fluorophore. As such, the reactive moiety (*i.e.*, carbamate), ammonium group and fluorophore can be integrated into one molecule and simultaneously it can match the aforementioned two criteria. To further reduce the rigidity of the molecule and to enhance interacting flexibility, a methylene group was set between the methylated ammonium group and *ortho*-carbon of phenolic hydroxy to enhance interacting flexibility. In addition, we also employed substrates with electron-donating and electron-withdrawing groups to tune the selectivity toward AChE for comparison.

With this in mind, a control probe (**CP**) and probes 1–10 (**P1–P10**) were synthesized by incorporating the designed substrates into excellent fluorochrome resorufin bearing different substituents (Scheme 2A and B). The detection mechanism of the probes with AChE is based on the hydrolysis of dimethyl carbamate followed by 1,6-rearrangement-elimination, accompanied by the release of resorufin (Scheme 2C). The detailed

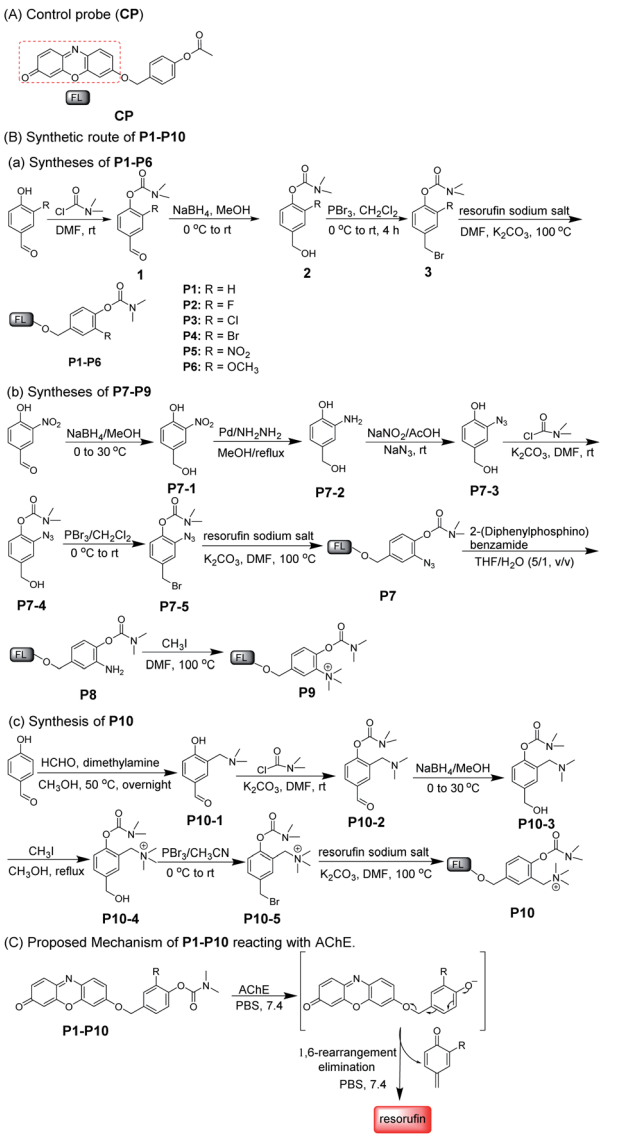

Scheme 2 The syntheses and chemical structures of CP and **P1–P10**. (A) A control probe (**CP**). (B) Syntheses of fluorogenic probes (**P1–P10**) for the activity of AChE. (C) Proposed mechanism of the probes reacting with AChE.

Table 1 Photophysical properties of the control probe (**CP**), fluorogenic probes (**P1–P10**) and resorufin

Compd	λ_{ex}[a] (nm)	ε[b] (10^4)	λ_{em}[c] (nm)	Φ[d]	$\varepsilon \times \Phi$[e]	Compd	λ_{ex}[a] (nm)	ε[b] (10^4)	λ_{em}[c] (nm)	Φ[d]	$\varepsilon \times \Phi$[e]
CP	480	1.03	582	0.006	61.8	**P6**	475	1.50	582	0.009	135
P1	480	1.14	582	0.020	228	**P7**	480	0.88	582	0.005	44
P2	479	0.95	582	0.018	171	**P8**	475	1.51	582	0.003	45.3
P3	485	0.84	582	0.011	92.4	**P9**	480	2.13	582	0.008	170.4
P4	477	1.34	582	0.020	268	**P10**	478	2.30	582	0.008	184
P5	480	1.16	582	0.013	150.8	Resorufin[d]	571	5.69	582	0.75	42675

[a] Maximum absorbance peak. [b] Molar absorptivity of the corresponding absorbance peak (M^{-1} cm^{-1}). [c] Emission peak. [d] Fluorescence quantum yield (QY, Φ) was measured using resorufin as a standard ($\Phi = 0.75$ in deionized water)[18] [e] Brightness $= \varepsilon \times \Phi$. All spectral properties were acquired in PBS buffer (pH 7.4).

syntheses, characterization, and photophysical properties of all the compounds are given in Table 1 and the ESI.†

Results and discussion

Specificity of probes (CP and P1–P10) toward AChE

We first investigated the specificity of the probes (**CP** and **P1–P10**) toward AChE, BChE and CE. As shown in Fig. 1a and b, S1 and S2,† acetyl unit-containing **CP** can have a faster response to CE than BChE and AChE. Under the same conditions, the reaction of **CP** with CE has the highest fluorescence enhancement, and the fluorescence enhancement of **CP** with BChE is almost as the same as that of **CP** with AChE, clearly demonstrating that such AChE probes with the acetyl unit are interfered by CE and BChE. Thus, the acetyl unit is not suitable as a recognition moiety for selectively detecting the activity of AChE. Next, the reactivity of **P1–P10** with different substituted

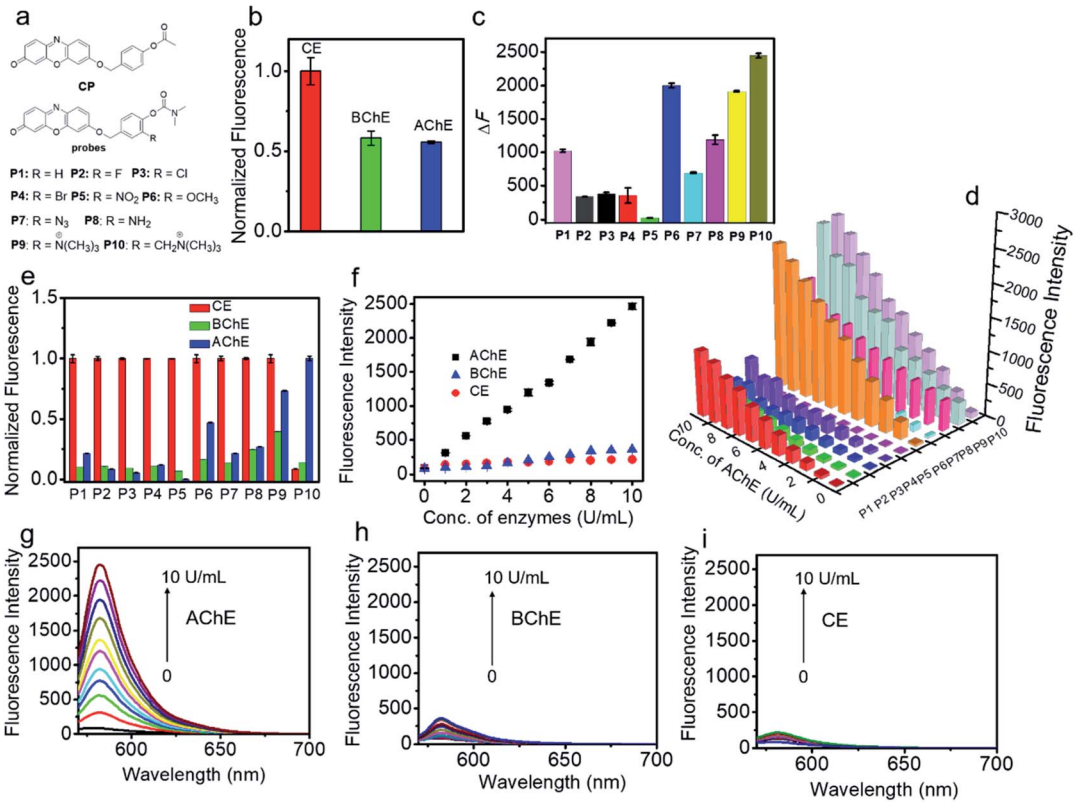

Fig. 1 (a) Chemical structures of CP and **P1–P10**. (b) Normalized fluorescence intensity of CP (5 μM) reacting with CE, BChE and AChE at 0.1 U mL^{-1} for 0.5 h at 37 °C in PBS buffer (pH 7.4), respectively. (c) Fluorescence response of **P1–P10** (5 μM) reacting with AChE (10 U mL^{-1}) for 5 h at 37 °C in PBS buffer (pH 7.4), respectively. ΔF is the fluorescence intensity difference after and before the reaction. (d) Fluorescence response of **P1–P10** (5 μM) reacting with AChE (0–10 U mL^{-1}) for 5 h at 37 °C in PBS buffer (pH 7.4), respectively. (e) Normalized fluorescence intensity of **P1–P9** (5 μM) reacting with CE (1 U mL^{-1}), BChE (10 U mL^{-1}), and AChE (10 U mL^{-1}), and P10 reacting with CE (10 U mL^{-1}), BChE (10 U mL^{-1}) and AChE (10 U mL^{-1}) for 5 h at 37 °C in PBS buffer (pH 7.4), respectively. (f) Fluorescence response of P10 (5 μM) toward CE, BChE and AChE (10 U mL^{-1}) for 5 h at 37 °C in PBS buffer (pH 7.4), respectively. Concentration dependent response of P10 toward (g) AChE (0–10 U mL^{-1}), (h) BChE (0–10 U mL^{-1}), and (i) CE (0–10 U mL^{-1}) for 5 h at 37 °C in PBS buffer (pH 7.4). The results are expressed as mean ± SD ($n = 3$). $\lambda_{ex/em} = 550/582$ nm.

units for AChE was tested. As shown in Fig. 1a, c, d, and S3,† except for **P5**, **P1–P4** and **P6–P10** all have different reactivities toward AChE, among which **P10** displays the highest fluorescence intensity. Besides, compared to **P1**, **P2–P8** having different electron-withdrawing and -donating groups show less or higher reactivity toward AChE. **P9** and **P10**, which have methylated ammonium groups, also showed better reactivity with AChE than **P1**. Moreover, increased reactivity toward AChE and reduced reactivity toward CE were observed for **P9**, which indicates that methylated ammonium may play an important role in the control of probe specificity for AChE. In addition, by introducing a methylene group between the methylated ammonium group and the *ortho*-carbon of the phenolic hydroxyl group in **P9**, **P10** shows better reactivity for AChE than **P9**. These data demonstrated that our design is rational and effective, and this observation may also provide and promote a better understanding of the design of reacting units for AChE detection. As seen in Fig. 1e–i, S3 and S4,† we further investigated the specificity of **P1–P10** for AChE over BChE and CE. We found that **P1–P9** have not only better reactivity toward AChE but also superior reactivity toward CE. However, surprisingly, **P10** shows the best reactivity and specificity toward AChE, which can effectively eliminate interference from BChE and CE. Compared to the rigidity of **P9**, which reduces its specificity, the interacting flexibility of **P10** indeed increases its specificity for AChE over BChE and especially CE.[52] To better understand this difference between **P9** and **P10** in terms of specificity toward AChE, BChE and CE, kinetic parameters were measured. As shown in Fig. S5, Tables S1 and S2,† **P10** shows a higher affinity and kinetic efficiency for AChE ($K_m = 4.87$ μM; $k_{cat}/K_m = 5.3 \times 10^4$ s^{-1} M^{-1}) than **P9** ($K_m = 6.45$ μM; $k_{cat}/K_m = 3.7 \times 10^4$ s^{-1} M^{-1}), whereas **P9** shows higher affinity and kinetic efficiency for CE ($K_m = 1.01$ μM; $k_{cat}/K_m = 5.9 \times 10^6$ s^{-1} M^{-1}) than **P10** for CE ($K_m = 29.57$ μM; $k_{cat}/K_m = 6.8 \times 10^3$ s^{-1} M^{-1}). The kinetic study is roughly in accordance with the fluorescence responses of **P9** and **P10** toward AChE, BChE and CE. These results all further demonstrate that our approach to designing a specific substrate for AChE detection without interference from BChE and CE is reasonable and effective. Considering its excellent specificity for AChE, **P10** was chosen as a candidate for subsequent studies.

Spectroscopic characteristics of P10

P10 itself exhibited an absorption maximum at 478 nm with negligible emission ($\Phi \approx 0.008$, Fig. S6† and Table 1), but the reaction mixture of **P10** with AChE showed a dramatic absorption peak shift to 571 nm with a distinct color change from colorless to pink, accompanied by a significant fluorescence enhancement at 582 nm with orange emission. This noticeable change in the spectroscopic signal benefits the sensitive detection of AChE. Subsequently, the reaction conditions (pH, temperature, and time) were optimized. As shown in Fig. S7 and S8,† the fluorescence intensity reached a maximum within the buffer solution (pH 7.4) during incubation at 37 °C, indicating the high applicability of **P10** under physiological conditions.

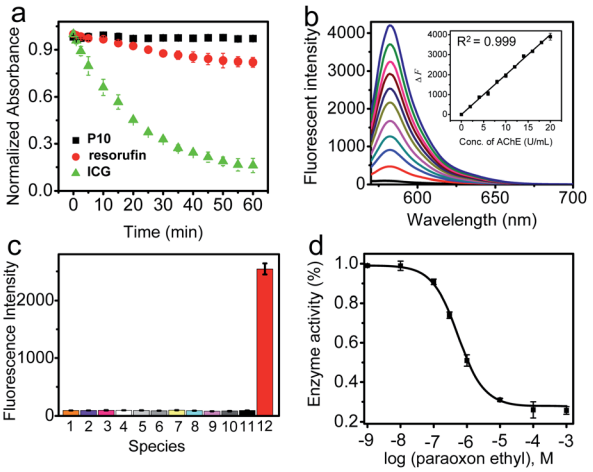

Fig. 2 (a) Photostability of **P10**, resorufin and ICG in PBS detected *via* absorbance spectra. The samples (all at 5 μM) were continuously irradiated with a light source. The power density was 39 mW cm^{-2}. (b) Linear relationship between ΔF and AChE concentration (0–20 U mL^{-1}) for 5 h at 37 °C in PBS buffer (pH 7.4). ΔF is the fluorescence difference after and before the reaction. (c) Fluorescence response of **P10** (5 μM) to different enzymes, including (1) a blank; (2) xanthine oxidase (10 mU mL^{-1}); (3) tyrosinase (10 U mL^{-1}); (4) MAO-A (10 μg mL^{-1}); (5) MAO-B (10 μg mL^{-1}); (6) β-glucosidases (10 U mL^{-1}); (7) trypsin (10 μg mL^{-1}); (8) ALP (10 U mL^{-1}); (9) apyrase (10 U mL^{-1}); (10) HSA (10 μM); (11) BSA (10 μM); and (12) AChE (10 U mL^{-1}) for 5 h at 37 °C in PBS buffer (pH 7.4). (d) Inhibitory activity of **P10** against paraoxon ethyl (10^{-9}–10^{-3} M). $\lambda_{ex/em}$ = 550/582 nm. The results are expressed as mean ± SD.

The time course studies revealed that higher concentrations of the probe will lead to faster responses and stronger fluorescence than lower concentrations. As shown in Fig. 2a, the photostability of **P10** was also tested. Compared to the clinically approved molecular dye indocyanine green (ICG), the fluorophore of resorufin used in our experiments and **P10** both have higher photostability.

Under the optimized conditions, the fluorescence response of **P10** to AChE was studied over a wide concentration range (Fig. 2b). A close-correlation between the concentration of AChE and emission intensity was observed, and good linearity was obtained at concentrations of 0–20 U mL^{-1}. The linear regression equation is $\Delta F = 200 \times C\,(\mathrm{U\,mL^{-1}}) - 1.5$, with a correlation coefficient of 0.999. The detection limit ($k = 3$)[53] was calculated to be 0.017 U mL^{-1}, which is lower than the physiological activity (approximately 5.0 U mL^{-1}).[54]

Next, selectivity assay of **P10** over other potential interfering species was performed, such as some enzymes [xanthine oxidase, tyrosinase, monoamine oxidase A (MAO-A), monoamine oxidase B (MAO-B), β-glucosidases, trypsin, alkaline phosphatase (ALP) and apyrase], human serum albumin (HSA), bovine serum albumin (BSA), some inorganic salts (KCl, $MgCl_2$, $CaCl_2$ and $ZnCl_2$), glucose, vitamin C, some amino acids (tyrosine, cysteine, glycine, glutamic acid, arginine, alanine and lysine), glutathione, urea and some reactive oxygen species (H_2O_2, ClO^-, TBHP, $^{\bullet}OH$, $TBO^{\bullet}$, $O_2^{\bullet-}$, $^1O_2$, $ONOO^-$, NO_2, CO and NO) (Fig. 2c, S9 and S10†). **P10** shows the most substantial fluorescence response toward AChE, whereas its response with

the other potential interfering species showed no significant emission enhancement. These results indicate that **P10** is suitable for the selective detection of AChE within complex biological contexts.

To evaluate the sensing mechanism, the reaction product of **P10** and AChE was analyzed by electrospray ionization (ESI) mass spectrometry and high-performance liquid chromatography (HPLC). As shown in Fig. S11,† the released resorufin was confirmed by an ESI peak of resorufin at 212.00 $[M - H]^-$. Moreover, HPLC analysis further verified the generation of resorufin as a reaction product (Fig. S12†). The peak deceased at 5.73 min indicating **P10** in the HPLC spectrum and was accompanied by the appearance of a new peak at 10.52 min representing resorufin. These results both clearly suggest that the reaction product was generated from the reaction of **P10** and AChE.

Based on the recognition ability of **P10** toward AChE, we investigated the applicability of **P10** for the inhibitor screening of AChE by IC_{50} value measurement. The IC_{50} value could be used to describe the inhibitory capacity of an inhibitor. As a known and effective inhibitor of AChE, paraoxon ethyl (PO) was selected as a candidate for this study.[1] In the inhibition assay, the paraoxon ethyl was mixed with AChE, and then **P10** was added. By measuring the fluorescence signal of **P10**, PO showed an IC_{50} value of 110 nM, which is roughly consistent with the reported reference (Fig. 2d and S13†).[55]

Fluorescence imaging of AChE activity within cells

The high specificity and sensitivity of **P10** make it possible to image AChE activity in living cells. Human embryonic kidney cells (HEK293 cells), mouse neuroblastoma cells (N2A cells), and human primary glioblastoma cells (U87MG cells) were chosen as model cell lines. Prior to the study, the potential toxicity of **P10** to cells was evaluated by the standard CCK-8 assay, and it showed high biocompatibility with all three cell lines (Fig. S14†). First, we compared the activity of AChE in different cells under the same conditions. We hypothesized that the penetrating ability of the probe into each cell is the same; the three cell lines show different fluorescence intensities (Fig. S15†); the strongest intensity was within U87 MG cells, moderate intensity is observed within N2A cells, and the weakest intensity is seen within HEK293 cells, indicating different expression levels of AChE in these cells, which can be further evidenced by the tested AChE activity in three cell lysates based on the Ellman method. Among them, U87MG cells might have the highest activity level of AChE. These results confirm that **P10** could be utilized for comparing the activity of AChE in different cells.

To further demonstrate the applicability of **P10** in the field of drug development, an inhibitory experiment was performed within U87MG cells. The untreated U87MG cells show no autofluorescence signals under imaging conditions, but the cells treated with **P10** show bright fluorescence in the cell cytosol (Fig. 3a and b), suggesting that **P10** has a good cell-permeability and possibly reacted with AChE within the cells. To verify that the fluorescence enhancement arises from the reaction of **P10** and AChE, cells were pretreated with PO, and then **P10** was added. In these cells, a low fluorescence signal was observed within the cell cytosol, compared to the **P10**-treated cells without the addition of an inhibitor. These results indicate that the probe **P10** could be employed to visualize the activity of AChE within living cells.

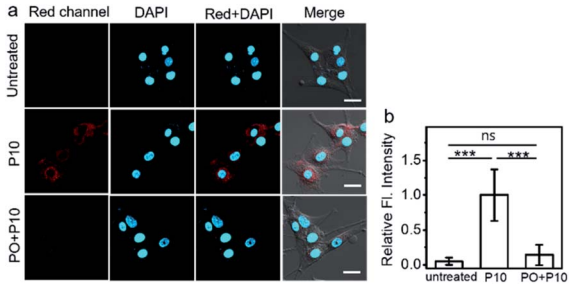

Fig. 3 (a) Fluorescence images of U87MG cells. (a) First row: cell only (untreated **P10** cells). Second row: cells treated with **P10** (5 μM) for 5 h at 37 °C. Third row: cells pretreated with 10 μM paraoxon ethyl (PO) for 1 h and then incubated with **P10** (5 μM) for 5 h at 37 °C. The red channel was collected in the range of 571–700 nm (ex. at 561 nm) and the DAPI channel was collected in the range of 415–550 nm (ex. at 405 nm), respectively. The third column displays merged images of red and DAPI channels. The fourth column displays merged images. (b) Relative fluorescence intensity in each cell. Data represent the mean ± SD. Statistical analysis was performed using one-way analysis of variance (ANOVA) followed by Tukey's *post hoc* test (***$p < 0.001$ and ns = non-significant). Scale bar: 20 μm.

In vivo and *ex vivo* visualization of AChE activity within the mice brains

Inspired by the capacity for imaging AChE activity in cells, **P10** was applied further to image AChE activity within a live mouse brain. For the *in vivo* brain imaging, **P10** was injected into the brain cerebral hemisphere and lateral ventricle sites. As shown in Fig. 4Aa–Ac, bright fluorescence was observed within the **P10**-treated mouse brain; compared to the PBS-treated mouse brain, representing the superior visualization ability of **P10** toward the activity of AChE in living biosystems.

Besides, an *ex vivo* imaging experiment was also performed (Fig. 4Ba). In this set, the mouse brain was first isolated and then treated with PBS (control), **P10**, and the inhibitor (PO) with **P10** (Fig. S16†). The PBS control set showed no autofluorescence signals under the experimental conditions (Fig. 4Bb, top), but the **P10** treated set showed bright fluorescence signals (Fig. 4Bb, middle). Moreover, we found significantly reduced fluorescence signals in the inhibitor-treated brain (Fig. 4Bb, bottom, Fig. 4Bc), suggesting that the fluorescence signal was derived from the reaction of **P10** with AChE in the mouse brain. The *in vivo* and *ex vivo* imaging results represent that **P10** has the capacity to selectively visualize AChE activity in living systems.

Furthermore, we attempted fluorescence-based AChE activity mapping within the healthy mouse brain by using **P10**. The isolated mouse brain was incubated with **P10**, and fluorescence images were recorded in the lambda (LA), left cerebral

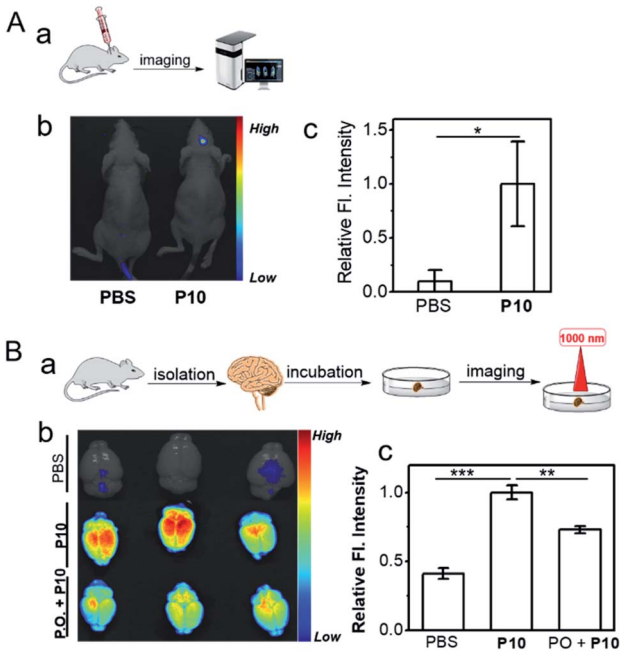

Fig. 4 (A) *In vivo* imaging AChE activity within the mice brains. (a) Schematic illustration of the *in vivo* animal study. **P10** was injected into a live mouse brain and the fluorescence signal was analyzed by using *in vivo* fluorescence microscopy. (b) *In vivo* whole-body fluorescence scanning images of the normal mouse after local treatment of PBS (control, pH 7.4) and **P10** (100 μM, PBS, pH 7.4) in the brain. The number of mice for each group is 3 ($n = 3$). (c) Fluorescence intensity plot from the images (head) in panel (b). (B) *Ex vivo* visualization of AChE activity within the mice brains. (a) Schematic illustration of the *ex vivo* animal study using *ex vivo* fluorescence microscopy. The normal mouse brain was isolated and then analyzed after treatment with **P10**. (b) *Ex vivo* whole-brain fluorescence scanning images of mouse brains after treatment with PBS, **P10** (100 μM), and **P10** with PO pretreatment. In this last set, PO (200 μM) was injected into the mouse brain 3 h before the injection of **P10** (100 μM). $n = 3$. (c) Fluorescence intensity plot from the images in panel (b). The brain samples were incubated with **P10** at 37 °C for 5 h. One-photon FTIS mode: $\lambda_{ex} = 530$ nm; $\lambda_{ex} = 570–640$ nm. Data represents the mean ± SD. Statistical analysis was performed by using one-way ANOVA followed by Tukey's *post hoc* test. (**$p < 0.01$ and ***$p < 0.001$).

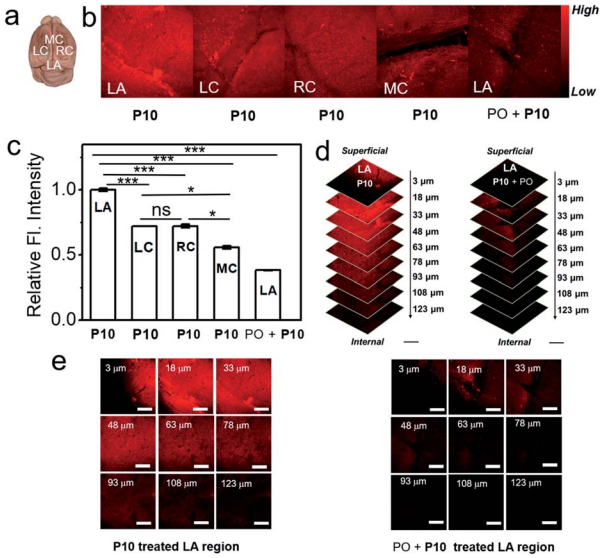

Fig. 5 Fluorescence images of normal brain tissue obtained by two-photon microscopy. (a) Mouse brain with an anatomical index of regions. LA, lambda; LC, left cerebral cortex; RC, right cerebral cortex; and MC, middle cortex. (b) Left four images: TPM images from the **P10**-treated (100 μM) mouse brain in the LA, LC, RC, and MC tissue regions. Right image: TPM fluorescence image of the **P10**-treated (100 μM) treated mouse brain in the LA region, which was pretreated with an inhibitor (PO, 200 μM). $n = 3$. (c) The intensity plot from the images in panel (b). (d and e) TPM tissue images of the mouse brain in the LA region at the indicated depth (3–123 μm, intervals of 15 μm) with the treatment of (left) **P10** and (right) **P10** with the pre-treated inhibitor. Scale bar: 200 μm. TPM images of each tissue were recorded after incubation with **P10** for 5 h at 37 °C. Two-photon excitation: $\lambda_{ex} = 1000$ nm; detection channel: $\lambda_{ex} = 565–675$ nm. Data represents the mean ± SD. Statistical analysis was performed using one-way ANOVA followed by Tukey's *post hoc* test (*$p < 0.05$ and ***$p < 0.001$).

cortex (LC), right cerebral cortex (RC), and middle cortex (MC) regions by using three-dimensional (3D) two-photon microscopy (TPM).[56] As shown in Fig. 5, the fluorescence intensity in the LA region of the brain is the strongest; the LC regions has moderate fluorescence, which is almost as the same as that in the RC region; the MC region shows the weakest fluorescence intensity indicating that the LA region may have the highest AChE level in the brain (Fig. 5b and c). A *Z*-sectioned two-photon scan of **P10** treated brain tissue displays a high tissue permeability and deep tissue imaging ability of **P10** (Fig. 5d and S17–S21†). The inhibitory experiment in the LA region suggested that the fluorescence signal was derived from AChE activity (Fig. 5e). The distribution data might provide important information on AChE activity in translational studies. All the tissue imaging results suggest that **P10** can visualize the activity of AChE in the brain, further extending the application of this probe in biological studies.

Conclusions

In summary, we have developed a new approach for the design of substrates to detect the activity of AChE by combining dimethylcarbamate choline with a self-immolative scaffold (4-hydroxybenzyl alcohol). On this basis, a series of probes were synthesized and a promising compound was found, **P10**, which shows high selectivity and sensitivity toward AChE, with no interference from BChE and CE. The high specificity of this probe was successfully confirmed by imaging AChE in different cells. In addition, this probe can monitor AChE activity and map the distribution of AChE activity in the normal mouse brain. The acquired results in this work might be of great significance for studying AChE in various research fields. These results successfully proved that our approach to designing a specific substrate for AChE detection is rational and effective. Moreover, such a substrate might be used to develop better AChE probes with different spectroscopic properties for better elucidating AChE activity in complex biosystems and could also provide a strategy for developing specific substrates for other enzymes.

Conflicts of interest

The authors declare no competing financial interests.

Acknowledgements

All of the experiments performed with mice were carried out in accordance with the National Institute of Health Guide for the Care and Use of Laboratory Animals (NIH Publications No. 80-23) revised in 1996 and protocols approved by the Institutional Animal Care and Use Committee of Kyung Hee University [KHUASP(SE)-19-002]. J. Y. thanks the National Research Foundation of Korea (NRF), which was funded by the Korea government (MSIP) (No. 2012R1A3A2048814). D. K. acknowledges the financial support from the NRF of Korea (No. 2019-M3A9H1103783, No. 2018-M3A9H3021707, and No. 2018-R1A6A1A03025124). O. M. S. acknowledges the support from the Medical Research Center Program through the NRF of Korea funded by the Ministry of Science and ICT (No. 2017-R1A5A2014768). H. M. M. thanks the National Natural Science Foundation of China (No. 21820102007).

Notes and references

1 D. M. Quinn, *Chem. Rev.*, 1985, **85**, 955–979.
2 K. D. Green, M. Fridman and S. Garneau-Tsodikova, *Chembiochem*, 2009, **10**, 2191–2194.
3 G. Sberna, J. Valero-Saez, Q. X. Li, C. Czech, K. Beyreuther, C. L. Masters, C. A. McLean and D. H. Small, *J. Neurochem.*, 1998, **71**, 723–731.
4 M. G. Savelieff, G. Nam, J. Kang, H. J. Lee, M. Lee and H. M. Lee, *Chem. Rev.*, 2019, **119**, 1221–1322.
5 E. Krejci, I. M. P. Valenzuela, R. Ameziane and M. Akaaboune, *J. Biol. Chem.*, 2006, **281**, 10347–10354.
6 L. Silman and J. L. M. Sussman, *J. Neurochem.*, 2017, **142**, 19–25.
7 H. Sorep and S. A. Seidman, *Nat. Rev. Neurosci.*, 2001, **2**, 294–302.
8 M. Behra, X. Cousin, C. Bertrand and J. L. Vonesch, *Nat. Neurosci.*, 2002, **5**, 111–118.
9 X. J. Zhang, L. Yang, Q. Zhao, J. P. Caen, H. Y. He, Q. H. Jin, L. H. Guo, M. Alemany, L. Y. Zhang and Y. F. Shi, *Cell Death Differ.*, 2002, **9**, 790–800.
10 T. Han and G. Wang, *J. Mater. Chem. B*, 2019, **7**, 2613–2618.
11 R. Jin, Z. Xing, D. Kong, X. Yan, F. M. Liu, Y. Gao, P. Sun, X. Liang and G. Lu, *J. Mater. Chem. B*, 2019, **7**, 1230–1237.
12 S. Sabelle, P. Y. Renard, K. Pecorella, S. D. Suzzoni-Dezard, C. Creminon, G. Gressi and C. Mioskiowski, *J. Am. Chem. Soc.*, 2002, **124**, 4874–44880.
13 H. Wang, J. Wang, C. Timchalk and Y. Lin, *Anal. Chem.*, 2008, **80**, 8477–8484.
14 D. Lu, J. Wang, L. Wang, D. Du, C. Timchalk, R. Barry and Y. Lin, *Adv. Funct. Mater.*, 2011, **21**, 4371–4378.
15 D. Liu, W. Chen, J. Wei, X. Li, Z. Wang and X. Jiang, *Anal. Chem.*, 2012, **84**, 4185–4191.
16 G. Zhou, F. Wang, H. Wang, S. Kambam, X. Chen and J. Yoon, *ACS Appl. Mater. Interfaces*, 2013, **5**, 3275–3280.
17 K. Gu, W. Qiu, Z. Guo, C. Yan, S. Zhu, D. Yao, P. Shi, H. Tian and W. H. Zhu, *Chem. Sci.*, 2019, **10**, 398–405.
18 J. Ohata, K. J. Bruemmer and C. J. Christopher, *Acc. Chem. Soc.*, 2019, **52**, 2841–2848.
19 H. Li, Y. Li, Q. Yao, J. Fan, W. Sun, S. Long, K. Shao, J. Du, J. Wang and X. Peng, *Chem. Sci.*, 2019, **10**, 1619–1625.
20 X. Li, X. Gao, W. Shi and H. Ma, *Chem. Rev.*, 2014, **114**, 590–659.
21 J. Zhang, X. Chai, X. P. He, H. J. Kim, J. Yoon and H. Tian, *Chem. Soc. Rev.*, 2019, **48**, 683–722.
22 R. Wang, J. Chen, J. Gao, J. A. Chen, G. Xu, T. Zhu, X. Gu, Z. Guo, W. H. Zhu and C. Zhao, *Chem. Sci.*, 2019, **10**, 7222–7227.
23 M. Kawatanti, K. Yamamoto, D. Yamada, M. Kamiya, J. Miyakawa, Y. Miyama, R. Kojima, T. Morikawa, H. Kume and Y. Urano, *J. Am. Chem. Soc.*, 2019, **141**, 10409–10416.
24 K. Li, W. Qiu, J. Li, Xi. Chen, Y. Hu, Y. Gao, D. Shi, X. Li, H. Lin, Z. Hu, G. Dong, C. Sheng, B. Jiang, C. Xia, C. Y. Kim, Y. Guo and J. Li, *Chem. Sci.*, 2020, **11**, 7292–7301.
25 D. Wang and B. Z. Tang, *Acc. Chem. Soc.*, 2019, **52**, 2559–2570.
26 H. W. Liu, K. Li, X. X. Hu, L. Zhu, Q. Rong, Y. Liu, X. B. Zhang, J. Hasserodt, F. Li. Qu and W. Tan, *Angew. Chem., Int. Ed.*, 2017, **56**, 11788–11792.
27 Y. Li, H. Song, C. Xue, Z. Fang, L. Xiong and H. Xie, *Chem. Sci.*, 2020, **11**, 5889–5894.
28 Y. Zhang, C. Yan, C. Wang, Z. Guo, X. Liu and W. H. Zhu, *Angew. Chem., Int. Ed.*, 2020, **59**, 9059–9066.
29 M. Mao, F. Yu, C. Lv, J. Choo and L. Chen, *Chem. Soc. Rev.*, 2017, **46**, 2237–2271.
30 X. Zhen, J. Zhang, J. Huang, C. Xie, Q. Miao and K. Pu, *Angew. Chem., Int. Ed.*, 2018, **57**, 7804–7808.
31 F. Feng, Y. Tang, S. Wang, Y. Li and D. Zhu, *Angew. Chem., Int. Ed.*, 2007, **46**, 7882–7886.
32 J. Chen, D. Liao, Y. Wang, H. Zhou, Y. Li and C. Yu, *Org. Lett.*, 2013, **15**, 2132–2135.
33 B. Wang, H. Wang, F. Wang, G. Zhou, Y. Wang, S. Kambam and X. Q. Chen, *Bioorg. Med. Chem. Lett.*, 2014, **24**, 552–555.
34 S. Liao, W. Han, H. Ding, D. Xie, H. Tan, S. Yang, Z. Wu, G. Shen and R. Yu, *Anal. Chem.*, 2013, **85**, 4968–4973.
35 Y. Zhang, Y. Cai, Z. Qi, L. Lu and Y. Qian, *Anal. Chem.*, 2013, **85**, 8455–8461.
36 D. Liao, J. Chen, H. Zhou, Y. Wang, Y. Li and C. Yu, *Anal. Chem.*, 2013, **85**, 2667–2672.
37 A. S. Y. Law, M. C. L. Yeung and V. M. M. Yan, *ACS Appl. Mater. Interfaces*, 2019, **11**, 4799–4808.
38 P. Zhang, C. Fu, Y. Xiao, Q. Zhang and C. Ding, *Talanta*, 2020, **208**, 120406–120416.
39 K. Cui, Z. Chen, Z. Wang, G. Zhang and D. Zhang, *Analyst*, 2011, **136**, 191–195.
40 Y. Zhang, W. Chen, D. Feng, W. Shi, X. Li and H. Ma, *Analyst*, 2012, **137**, 716–721.
41 S. Yoo and S. M. Han, *Chem. Commun.*, 2019, **55**, 14574–14577.
42 S. Y. Liu, H. Xiong, J. Q. Yang, S. H. Yang, Y. Li, W. Yang and G. F. Yang, *ACS Sens.*, 2018, **3**, 2118–2128.
43 X. Wang, P. Li, Q. Di, C. Wu, W. Zhang and B. Tang, *J. Am. Chem. Soc.*, 2019, **141**, 2061–2068.
44 J. Ma, T. Si, C. Yan, Y. Li, Q. Li, X. Lu and Y. Guo, *ACS. Sens.*, 2020, **5**, 83–92.

45 P. M. Potter, C. A. Pawlik, C. L. Morton, C. W. Naeve and M. K. Danks, *Cancer Res.*, 1998, **58**, 2646–2651.
46 D. J. Burkhart, B. L. Barthel, G. C. Post, B. T. Kalet, J. W. Nafie, R. K. Shoemaker and T. H. Koch, *J. Med. Chem.*, 2006, **49**, 7002–7012.
47 D. J. Horgan, E. C. Webb and B. Zerner, *Biochim. Biophys. Res. Commun.*, 1966, **23**, 23–28.
48 J. L. Sussman, M. Harel, F. Frolow, C. Oefner, A. Goldman, L. Toker and L. Silman, *Science*, 1991, **253**, 872–879.
49 H. Dvir, L. Silman, M. Harel, T. L. Rosenberry and J. L. Sussman, *Chem.-Biol. Interact.*, 2010, **187**, 10–22.
50 S. Gnaim and D. Shabat, *Acc. Chem. Soc.*, 2014, **47**, 2970–2984.
51 J. Yan, S. Lee, A. Zhang and J. Yoon, *Chem. Soc. Rev.*, 2018, **47**, 6900–6916.
52 B. M. Liederer and R. T. Borchardt, *J. Pharm. Sci.*, 2006, **95**, 1177–1195.
53 X. Wu, W. Shi, X. Li and H. Ma, *Angew. Chem., Int. Ed.*, 2017, **56**, 15319–15323.
54 A. Alvarez, R. Alarco, C. Opazo, E. O. Campos, F. J. Munoz, F. H. Caldeo, F. Dajas, M. K. Gentry, B. P. Doctor, F. G. Demello and N. C. Inestrosa, *J. Neurosci.*, 1998, **18**, 3213–3223.
55 F. Verdin-Betancourt, M. Figueroa, M. D. L. Lopez-Gonzalez, E. Gomez, Y. Y. Bernal-Hernandez, A. E. Rojas-Garcia and A. Sierra-Santoyo, *Sci. Rep.*, 2019, **9**, 14758.
56 J. Mutze, V. Iyer, J. J. Macklin, J. Colonell, B. Karsh, Z. Petrasek, P. Schwille, L. L. Looger, L. D. Lavis and T. D. Harris, *Biophys. J.*, 2012, **102**, 934–944.